

# An Immersed Domain Method for Fluid-Structure Interaction with Contact

Maria Giuseppina Chiara Nestola<sup>[0000-0002-5700-0306]</sup>,  
Patrick Zulian<sup>[0000-0002-5822-3288]</sup>, Diego Rossinelli<sup>[0000-0003-1600-4068]</sup>, and  
Rolf Krause<sup>[0000-0001-5408-5271]</sup>

## 1 Introduction

Fluid-structure interaction (FSI) analysis has gained prominence across fields like aerodynamics, geophysics, and biomedicine due to the complex interplay between fluids and solids. A prime example of biomedical application is the dynamic behavior of cardiac valves.

Located within the heart, these valves regulate blood flow between chambers and major vessels. The aortic valve, in particular, controls blood flow from the heart to the body. Composed of three triangular leaflets, it opens and closes rhythmically to ensure efficient blood pumping and prevent backflow. When valves malfunction, they often require replacement with artificial or biological prosthetics to restore normal function. Simulating the dynamics of a native aortic valve or of its replacement during the entire cardiac cycle requires a computational framework able to resolve: 1) the fluid-structure interaction of the blood with the three leaflets and aortic root; 2) the elastodynamics of the contact between the tissues.

In the literature, several approaches have been developed for FSI simulations, which are divided into two main families: boundary-fitted and embedded methods.

In boundary-fitted methods, the Navier–Stokes equations are typically formulated in an Arbitrary Lagrangian Eulerian (ALE) framework. While the ALE method offers accurate fluid-solid interface representation, it can suffer from grid distortion due to

---

Maria G. C. Nestola,  
Università della Svizzera italiana, Euler institute, Lugano, CH, e-mail: nestom@usi.ch

Patrick Zulian  
Università della Svizzera italiana, Euler institute, Lugano, and UniDistance Suisse, Brig, CH, e-mail: patrick.zulian@usi.ch

Diego Rossinelli  
Stanford University, California, USA e-mail: rossinel@stanford.edu

Rolf Krause  
KAUST, Thuwal, KSA, and UniDistance Suisse, Brig, CH, e-mail: rolf.krause@kaust.edu.sa

large deformations and rotations. This compromises numerical stability and solution accuracy. Heart valve simulations are particularly challenging as maintaining high mesh quality during valve closure becomes computationally demanding.

Baaijens et al. proposed a *Fictitious Domain/Mortar Element Method* (FD/ME) for imposing the continuity of the velocities at the FSI interface [1]. This approach was generalized by Hesch et al. [4] for enforcing the velocity constraint over the entire overlapping region between fluid and solid domains, providing a fully discrete method that is unconditionally stable. The mortar method relies on the enforcement of weak-equality conditions between a master (mortar) discretization and a slave (non-mortar) discretization using the method of Lagrange multipliers. The Lagrange multiplier is typically associated with the slave discretization. To prevent penetration among leaflets, Kamensky et al. [5] employed a penalty method for enforcing the contact constraints. The penalty method has limitations in scenarios with high-pressure gradients developing in thin-structure applications like heart valves. To overcome such limitations, this work presents an immersed domain fluid-structure-contact interaction approach capable of simulating complex materials and flow patterns. The main contributions of the present work are the following:

1. we present an immersed domain method (IDM) for FSI with an accurate and stable resampling of fields across the fluid and the solid domains, which may feature complex 3D geometries;
2. the contact problem is solved with a mortar-based approach for simulating large deformations without requiring penalty parameter tuning;
3. we perform numerical simulations of a bio-prosthetic aortic heart valve with fiber-reinforced leaflets, a linear elastic rigid stent, and a hyperelastic and isotropic aortic root. A lumped model is coupled with the three-dimensional model of the aorta to reproduce the physiological pressure gradient. This allows analyzing the spatial distribution of the stresses during the entire heartbeat.

## 2 Fluid structure contact interaction (FSCI) formulation

The proposed FSCI coupling strategy is based on a mortar approach to treat both FSI [4] and contact constraints. We base our implementation on the resampling framework presented in [8], where we address the challenges of detecting intersections between arbitrarily distributed finite element meshes. In the spirit of the IDM, the coupling between the fluid flow and the elastic structure is established in the form of a vector constraint enforcing the continuity of velocities over the entire overlapping region  $\Omega_{FSI} = \Omega_s^t \cap \Omega_f$ , *i.e.*,  $\Omega_{FSI} = \Omega_s^t$ :

$$\mathbf{v}_f - \dot{\mathbf{u}}_s = \mathbf{0} \quad \text{in } \Omega_{FSI}, \quad (1)$$

where  $\Omega_f$  is the fluid domain,  $\Omega_s^t$  is the solid current configuration at time  $t$ ,  $\mathbf{v}_f$  is the fluid velocity field and  $\dot{\mathbf{u}}_s$  is the solid velocity field.

We abbreviate the function spaces definition  $V_k = V(\Omega_k)$ , and use  $f$  and  $s$  subscripts to refer to fluid and solid, respectively. With  $\Gamma_c \subseteq \partial\Omega_s^t$  we describe the a priori unknown time-dependent contact boundary. The variational formulation of the FSI contact problem reads:

$\forall t \in (0, T]$  find  $(\mathbf{v}_f \in \mathbf{V}_f, p_f \in Q_f, \mathbf{u}_s \in \mathbf{V}_s, \theta_c \in V_c, \lambda_{FSI} \in \mathbf{V}_{FSI})$  such that

$$\int_{\Omega_f} \rho_f (\dot{\mathbf{v}}_f + [(\mathbf{v}_f \cdot \nabla) \mathbf{v}_f]) \cdot \boldsymbol{\zeta}_f dV + \int_{\Omega_f} \mu_f \nabla \mathbf{v}_f \cdot \nabla \boldsymbol{\zeta}_f dV + \quad (2)$$

$$\int_{\Omega_f} p_f \nabla \cdot \boldsymbol{\zeta}_f dV - \int_{\Omega_{FSI}} \lambda_{FSI} \cdot \boldsymbol{\zeta}_f dV = R_f(\boldsymbol{\zeta}_f), \quad (3)$$

$$\int_{\Omega_f} q_f \nabla \cdot \mathbf{v}_f dV = 0, \quad (4)$$

$$\int_{\Omega_s} \rho_\Delta \ddot{\mathbf{u}}_s \cdot \boldsymbol{\zeta}_s dV + \int_{\Omega_s} \mathbf{P}(\mathbf{u}_s) : \nabla \boldsymbol{\zeta}_s dV + \quad (5)$$

$$\int_{\Omega_{FSI}} \lambda_{FSI} \cdot \boldsymbol{\zeta}_s dV + \int_{\Gamma_c} [\boldsymbol{\zeta}_s] \cdot \mathbf{n}_c \theta_c dS = R_s(\boldsymbol{\zeta}_s),$$

$$\int_{\Omega_{FSI}} (\dot{\mathbf{u}}_s - \mathbf{v}_f) \cdot \boldsymbol{\mu}_{FSI} dV = 0, \quad (6)$$

$$\int_{\Gamma_c} ([\mathbf{u}_s] \cdot \mathbf{n}_c - g) \psi_c dS \leq 0, \quad (7)$$

$$\lambda_c g_c(\mathbf{u}_s) = 0, \quad (8)$$

$$\lambda_c \geq 0, \quad (9)$$

$$\boldsymbol{\tau}_c(\mathbf{u}_s) = 0. \quad (10)$$

are satisfied  $\forall (\boldsymbol{\zeta}_f \in \mathbf{V}_f, \boldsymbol{\zeta}_s \in \mathbf{V}_s, q_f \in Q_f, \boldsymbol{\zeta}_s \in \mathbf{V}_s, \psi_c \in V_c, \boldsymbol{\mu}_{FSI} \in \mathbf{V}_{FSI})$  for suitable spaces of fluid velocities  $\mathbf{V}_f$  and pressures  $Q_f$ , of structure displacements  $\mathbf{V}_s$ , of Lagrange multipliers of the contact conditions  $V_c$ , and FSI conditions  $\mathbf{V}_{FSI}$ , respectively. The scalar  $\rho_\Delta = \rho_s - \rho_f$  is the difference between the structure  $\rho_s$  and the fluid density  $\rho_f$  in [4],  $\mu_f$  is the fluid viscosity, the terms  $R_k(\boldsymbol{\zeta}_k)$  with  $k = \{f, s\}$  account for the Neumann boundary conditions and body forces, and  $\mathbf{P}(\mathbf{u}_s)$  is the first-Piola-Kirchhoff tensor.

Equation (6) prescribes the continuity of the velocity field over the overlapping region  $\Omega_{FSI}$ , and  $\lambda_{FSI}$  is the Lagrange multiplier associated with the FSI constraint. Here, the solid is the master discretization and the fluid is the slave one.

Equation (7) prescribes the non-penetration constraint where  $g_c$  is a measure for the distance between the master and slave surfaces potentially in contact,  $\mathbf{n}_c$  is the outward unit normal to the slave surface, and  $[\cdot]$  is the jump operator, measuring with  $[\mathbf{u}_s] = \mathbf{u}_s^M - \mathbf{u}_s^S$  the difference between the displacements on the master ( $M$ ) and slave ( $S$ ) surfaces. The roles  $M$  and  $S$  are assigned to each contact pair of leaflets at simulation set-up time. The contact is considered without friction, hence the tangential stress  $\boldsymbol{\tau}_c(\mathbf{u}_s)$  is expected to be zero (10). The complementarity condition

(8), and positiveness of the Lagrange multiplier (9) are associated with the inequality constraint (7). Equations (8)-(10) are satisfied point-wise.

### 3 Discretization and solution of the saddle-point problem

We discretize the fluid and solid sub-problems with linear finite elements  $\mathbb{P}_1$ . To allow  $\mathbb{P}_1 - \mathbb{P}_1$  discretization of fluid velocity and pressure, we used the Streamline–Upwind Petrov–Galerkin (SUPG) stabilization. Contact conditions are discretized using the mortar method with dual Lagrange multipliers. The time discretization scheme for the fluid sub-problem is a second-order Backward Differentiation Formula (BDF2), while for the solid sub-problem, we adopt a contact-stabilized Newmark scheme [7]. The FSI constraints are ensured by using  $L^2$ -projections as described in [2, 8], using dual Lagrange multipliers.

For the iterative solution of the highly non-linear system (2)-(6) we consider the linearized system of equations

$$\begin{bmatrix} \mathcal{H}_f(\mathbf{y}_f) & \mathbf{0} & \mathbf{D}^T \\ \mathbf{0} & \mathcal{H}_s(\mathbf{y}_s) & -\mathbf{B}^T \\ \mathbf{D} & -\mathbf{B} & \mathbf{0} \end{bmatrix} \begin{bmatrix} \delta \mathbf{y}_f \\ \delta \mathbf{y}_s \\ \delta \mathbf{y}_\lambda \end{bmatrix} = \begin{bmatrix} \mathbf{R}_f \\ \mathbf{R}_s \\ \mathbf{R}_\lambda \end{bmatrix}, \quad (11)$$

subject to  $\mathbf{T}_c \mathbf{y}_s \leq \mathbf{g}_c$  on  $\Gamma_c$ , where  $\mathbf{y}_s$ ,  $\mathbf{y}_f$  and  $\mathbf{y}_\lambda$ , are solution vectors and  $\delta$  is used to denote the corresponding increment of the fluid velocity, solid displacement, and Lagrange multiplier of the FSI constraints, respectively. With  $\mathbf{T}_c$  we encapsulate the mortar operator and normal-tangential coordinate transformation of the contact constraints. The residual/hessian pairs of the equations are  $\mathbf{R}_f, \mathcal{H}_f$  for the fluid (2),  $\mathbf{R}_s, \mathcal{H}_s$  for the solid (5), and  $\mathbf{R}_\lambda$  is the FSI velocity constraint (6), whereas  $\mathbf{B}$  and  $\mathbf{D}$  are the mortar matrices. Note that the Lagrange multiplier for the FSI problem is associated with the fluid discretization.

We solve (11) with a non-linear block-Gauss–Seidel method, where fluid and solid sub-problems can be solved independently in a staggered way. For each iteration  $l$  we perform the following steps:

1. we solve the elastodynamic equations subject to the linearized contact constraint  $\mathbf{T}_c \mathbf{y}_s \leq \mathbf{g}_c$ , using a non-smooth solution strategy (e.g., the semi-smooth Newton method) as described in [12]. Note that for solving the solid sub-problem we linearize the contact conditions in an outer loop and the constitutive non-linearities in an inner loop;
2. we solve the Navier-Stokes equations subject to the velocity constraint,  $\mathbf{D} \mathbf{y}_f^l = \mathbf{B} \mathbf{y}_s^{l-1}$ ;
3. we update the vector of Lagrange multipliers  $\mathbf{y}_\lambda$ .

This iterative procedure terminates at  $l = L$  when the *absolute convergence criterion*  $\|\mathbf{y}_\lambda^l - \mathbf{y}_\lambda^{l-1}\| < \epsilon_A$ , or the *relative convergence criterion*  $\|\mathbf{y}_\lambda^l - \mathbf{y}_\lambda^{l-1}\| / \|\mathbf{y}_\lambda^0\| < \epsilon_R$

are satisfied. Finally, the solid and the fluid variables are updated as  $\mathbf{y}_s^{n+1} = \mathbf{y}_f^L$ ,  $\mathbf{y}_f^{n+1} = \mathbf{y}_f^L$  and we proceed to the next time-step.

The combination of the non-smooth solution approach for addressing the non-linear contact problem and a stabilized time integrator scheme results in a stable and energy dissipative scheme. We emphasize that the use of a dissipative scheme for multi-body dynamic contact prevents energy blow-ups and artificial oscillations in contact stresses while preserving linear momentum [7]. Moreover, solving the contact problem with high accuracy results in only a negligible energy loss due to the moment of impact ( $< 2\%$ ) as reported in [3, 7].

### 3.1 Conservation properties of the contact algorithm

In this section, we investigate the conservation of angular momentum of the stabilized Newmark time integration scheme for contact dynamics. To this aim, we consider the two-dimensional problem introduced by Laursen et al. [9], which involves an elastic ball impacting a rigid surface. The ball has a diameter equal to  $D = 20$  units and is located in a square box with length  $H = 200$  units (see Fig. 1 (A)). The elastic ball impacts the rigid box under an angle of incidence  $\theta = \frac{\pi}{4}$  with an initial velocity  $\dot{u}_{sx} = \dot{u}_{sy} = 2$  units. The material properties of the ball are: Young's modulus,  $E = 10^2$ , Poisson ratio  $\nu = 0.001$ , and density  $\rho_s = 1.0$  units. The material properties of the square box are: Young's modulus,  $E = 10^6$ , Poisson ratio  $\nu = 0.001$ , and density  $\rho_s = 1.0$  units in agreement with [12]. The solid mesh consists of 6600 elements and 3800 nodes. We use a constant time step  $\Delta t = 0.1$  [s].

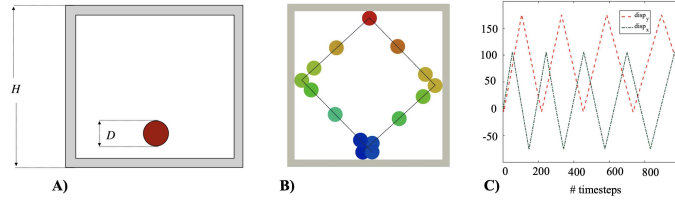


Fig. 1: (A) Geometric setting of the momentum conservation benchmark. (B) Snapshots of the trajectory of the circle at different time steps. (C) Displacement of the barycenter of the circle in the  $x$  and  $y$  direction.

Figures 1 (A) and (B) show the trajectory of the ball (colors refer to the magnitude of displacements) and the displacement field of its barycenter in both the  $x$  and  $y$  directions, respectively. As expected, the circle rebounds elastically at about  $\theta = \frac{\pi}{4}$  during the whole path in the box. A comparison between our results and those obtained with the classical Newmark method [9] reveals that our integration scheme allows for better conservation of both linear and angular momentum as already

pointed out in [6]. Indeed, Laursen et al. [9] showed that the classical Newmark time integrator preserves the rigid-body motion by reducing the impact angle, which becomes too flat. On the contrary, the modified Newmark integrator allows us to reproduce a diamond-shaped trajectory when fully solving the nonlinear contact problem with the desired accuracy.

## 4 FSI simulation of a bio-prosthetic heart valve

In this section, we present the results obtained by performing an FSI simulation of an idealized bio-prosthetic heart valve. We embed the solid domain (A) into a fluid and a rigid channel (B). As depicted in Fig. 2 the solid domain (A) comprises an aortic root and a bio-prosthetic aortic valve consisting of three leaflets and the surrounding rigid frame. We model the leaflets as an incompressible hyperelastic fiber-reinforced material, the aortic root as an incompressible hyperelastic Neo-Hookean material, and the rigid stent as an incompressible elastic linear material. Blood is modeled as an incompressible Newtonian fluid with density  $\rho_f = 1000$  [kg/m<sup>3</sup>], and viscosity  $\mu_f = 0.004$  [Pa · s].

We impose a velocity profile (see Fig. 2 (D)) on the inlet of the fluid domain, and no-slip conditions on the external surface. We couple the three-dimensional problem with a zero-dimensional Windkessel model to account for the peripheral artery system. In particular, the three-element Windkessel reads as follows [11]:

$$Q(t) = C \frac{dP_c(t)}{dt} + \frac{P_c(t)}{R_d} \quad (12)$$

$$P(t) = Q(t)R_p + P_c(t) \quad (13)$$

Here  $R_p$  is the proximal resistance,  $C$  is the compliance and  $R_d$  is the distal resistance,  $Q(t)$  represents the blood flow rate,  $P(t)$  is the proximal blood pressure and  $P_c(t)$  is distal pressure. By calibrating the three parameters of the Windkessel model, one can reproduce the experimental pressure profile as reported in Figure 2 (E). All the parameters are chosen in agreement with [10]. The inlet and the outlet rings of the aortic root are kept fixed in all directions, whereas a free stress boundary condition is imposed on the external surface. The fluid mesh consists of 844 864 elements and 149 567 nodes, whereas the solid mesh contains 850 136 elements and 191 523 nodes. A constant  $\Delta t = 0.001$  [s] is adopted for the time integration schemes for the two sub-problems.

Fig. 3 (A-D) shows snapshots of the velocity field at selected time instants of the same heartbeat. During the systolic acceleration, we observe a fully developed jet with a maximum velocity of about 2.0 [m/s] forming downstream of the aortic orifice and remaining confined to the core region of the aortic root. We point out that the SUPG scheme is not a physical model as its purpose is to provide sufficient algorithmic dissipation for a stable, consistent, and convergent numerical method.

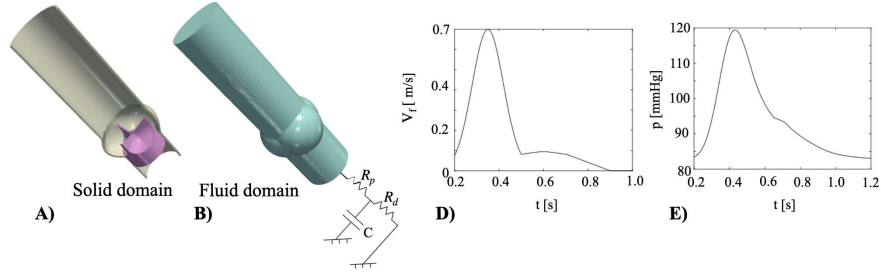


Fig. 2: (A) Bio-prosthetic valve in the aortic root (cut for visualization). (B) Fluid domain. (D) Velocity profile imposed at the inlet of the fluid domain and pressure profile (E) computed at the outlet with the Windkessel model.

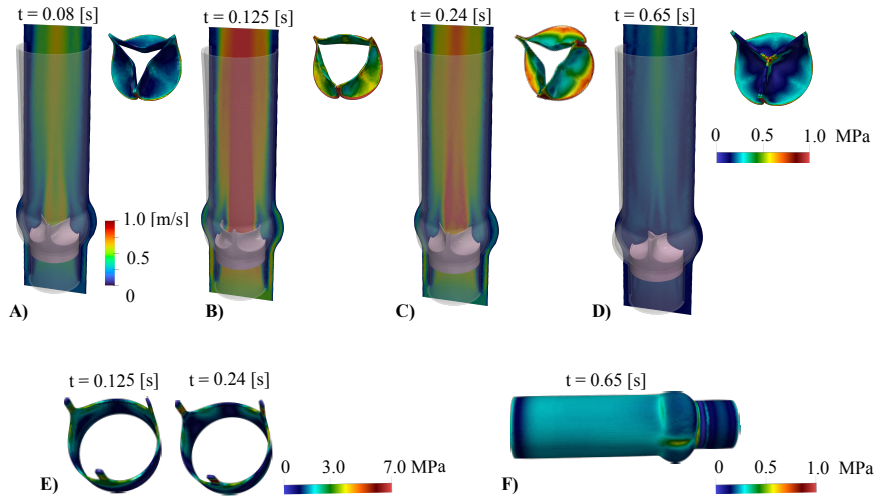


Fig. 3: Velocity field and von-Mises stress in the valve during opening (A-B) and closure (C-D) phases. The aortic root has been neglected for visualization purposes. Von-Mises stress in the stent (E) and in the aortic root (F).

Thus, the energy dissipation introduced by the SUPG scheme does not allow us to describe the turbulent systolic flow downstream of a bio-prosthetic aortic valve.

Fig. 3 (A-D) also shows snapshots of the spatial distribution of the von Mises stresses in the leaflets during the opening and closing phase. We observe that the stresses increase during the systolic acceleration of the blood and achieve a maximum of about 0.8 [MPa] in the central region of the leaflets during the early diastole (0.65 [s]). In the last picture (D) we observe high stresses in the contact region.

Fig. 3 (E) and (F) show the von Mises stresses in the rigid stent frame and the aortic root, respectively. We observe a stress concentration in the insertion of the stent, which represents the most solicited component.

## 5 Conclusions

We presented a fully coupled and variational immersed approach to FSCI for simulating viscous flows in a transitional regime and the contact problems between the immersed structures. This work is limited to piece-wise linear finite-element schemes for constructing the  $L^2$ -projection operator with machine precision. Future extensions include the use of higher-order schemes for the solid and the fluid problem, and turbulence modeling for describing the complex features of the aortic flow.

**Acknowledgments:** M.G.C.N thanks the SNSF (nr.: 197041). P.Z. thanks the USI-FIR, the SNSF (nr.: 215627), and the PASC XSES-FSI project.

## References

1. Baaijens, F.P.: A fictitious domain/mortar element method for fluid-structure interaction. *Int. J. Numer. Meth. Fl.* **35**(7), 743–761 (2001)
2. Boffi, D., Gastaldi, L.: A finite element approach for the immersed boundary method. *Comput. Struct.* **81**(8), 491–501 (2003)
3. Deuffhard, P., Krause, R., Ertel, S.: A contact-stabilized newmark method for dynamical contact problems. *International Journal for Numerical Methods in Engineering* **73**(9), 1274–1290 (2008)
4. Hesch, C., Gil, A., Carreño, A.A., Bonet, J., Betsch, P.: A mortar approach for fluid–structure interaction problems: Immersed strategies for deformable and rigid bodies. *Comput. Method Appl. M.* **278**, 853–882 (2014)
5. Kamensky, D., Hsu, M.C., Schillinger, D., Evans, J.A., Aggarwal, A., Bazilevs, Y., Sacks, M.S., Hughes, T.J.: An immersogeometric variational framework for fluid–structure interaction: Application to bioprosthetic heart valves. *Computer methods in applied mechanics and engineering* **284**, 1005–1053 (2015)
6. Krause, R., Walloth, M.: A time discretization scheme based on rothe’s method for dynamical contact problems with friction. *Computer Methods in Applied Mechanics and Engineering* **199**(1-4), 1–19 (2009)
7. Krause, R., Walloth, M.: Presentation and comparison of selected algorithms for dynamic contact based on the newmark scheme. *Applied Numerical Mathematics* **62**(10), 1393–1410 (2012)
8. Krause, R., Zulian, P.: A parallel approach to the variational transfer of discrete fields between arbitrarily distributed unstructured finite element meshes. *SIAM J. Sci. Comput.* **38**(3), C307–C333 (2016)
9. Laursen, T., Chawla, V.: Design of energy conserving algorithms for frictionless dynamic contact problems. *International Journal for Numerical Methods in Engineering* **40**(5), 863–886 (1997)
10. Nestola, M.G., Gizzi, A., Cherubini, C., Filippi, S.: Three-band decomposition analysis in multiscale fsi models of abdominal aortic aneurysms. *Int. J. Mod. Phys. C* **27**(02), 1650017 (2016)
11. Olufsen, M.S., Nadim, A.: - on deriving lumped models for blood flow and pressure in the systemic arteries. In: K. Bathe (ed.) *Computational Fluid and Solid Mechanics 2003*, pp. 1786 – 1789. Elsevier Science Ltd, Oxford (2003)
12. von Planta, C., Vogler, D., Zulian, P., Saar, M.O., Krause, R.: Solution of contact problems between rough body surfaces with non matching meshes using a parallel mortar method. *arXiv preprint arXiv:1811.02914* (2018)